RSC Advances

PAPERS

An Inorganic Anionic Polymer Filter Disc: Direct Crystallization of a Layered Silicate Nanosheet on a Glass Fiber Filter

Tomohiko Okada,[a] Kei Shimizu[a] and Tomohiko Yamakami[b]

Received 00th January 20xx,
Accepted 00th January 20xx

DOI: 10.1039/x0xx00000x

www.rsc.org/

An inorganic anionic polymer filter disc was successfully produced from heterogeneous nucleation reactions of layered silicate fine crystals on amorphous silica glass fibers. This hybrid material can be obtained only by immersing the silica fiber filter disc in an aqueous solution containing LiF, $MgCl_2$, and urea at 373 K for 48 h. Silica sol, which was partially dissolved from the silica fibers by hydrolysis of urea, was a source of the layered silicate. Firm immobilization of the layered silicate on the fiber silica was confirmed by immersing in aqueous LiCl solution (12 mM) for three weeks. The layered silicate crystals evenly covered the silica fibers while maintaining the original filter disc shape. Careful design of the layered silicate was performed by changing the molar LiF:$MgCl_2$:urea:SiO_2 ratio. The layered silicate on the fibers became thick on adding increasing amounts of LiF and $MgCl_2$. In addition, by increasing the amount of LiF, the negative charge density of the layered silicate increased, following the trend of caffeine adsorption in water. Furthermore, we found that the amount of urea added to the starting solution was important for preventing a loss in the mechanical strength of the fibers (e.g., fracture due to unnecessary dissolution of the silica fiber) and emerging side-reactions (e.g., polymerization of silica sol to yield spherical silica particles). The resulting layers of silicate on the filter disc acted as adsorption sites for both organic (methylene blue and benzylammonium) and inorganic (sodium, calcium, and europium) cationic species in water, as exemplified by batch and flow tests.

Introduction

Hybridization between functional units and solids with controlled and useful structure/morphology is important in various applications, including adsorption–separation, detection, and controlled release. Diverse strategies have been established for the production of multifunctional hybrid materials, including fabrication of core–shell particles,[1,2] occlusion of functional species into hollow spherical particles,[3,4] coating on a substrate,[5,6] and the use of epitaxial crystal growth[7–9]. Layered inorganic solids have been widely used as building blocks for molecularly controlled hybrids with well-defined 2D nanostructures,[10–16] because layered solids are made by nanometer-thick layers and by naturally assembling as layered stacks. Surface modification and pillaring via intercalation are promising methods for generating hybrids at a molecular level with the ability for molecular recognition (e.g., selective adsorption of a target molecule).[13,15] Owing to the structural versatility, by changing the nature and amount (or spatial density) of the interlayer building units, it is possible to tune the surface properties, including hydrophobicity, porosity, and affinity, with the target molecules.

In contrast, the desired shape and morphology of the inorganic layered solids have been considered for practical use through different crystallization processes, including sol-gel, hydrothermal, and solid-state reactions.[17–22] For flow systems, in particular, fine crystals are preferred owing to their rapid and thorough contact with the target molecules in the interlayer space for a short period. However, careful handling and transporting are required to avoid a pressure drop. "Direct" crystallization of inorganic layered materials has been reported as layered silicates,[24,25] layered titanosilicate[26] (an anionic inorganic polymer), and layered double hydroxides (LDHs, cationic inorganic polymers)[27–29] on bulk solid substrates, unlike *papier mache* (e.g., the Langmuir–Blodgett method[30] and layer-by-layer deposition technique[31–33]). The improved adherence to substrates over conventional colloidal deposition techniques (e.g., spin and dip-coatings) should be useful in supporting layered inorganic materials with molecular recognition capabilities. We have discovered that a hectorite-like layered silicate fine crystal (abbreviated as Hect, with the ideal formula $M_x(Mg_{6-x}Li_xSi_8O_{20}(OH)_4 \cdot nH_2O$, where M represents interlayer exchangeable cations), an anionic 2D

[a] *Department of Chemistry and Material Engineering, Faculty of Engineering, Shinshu University, Wakasato 4-17-1, Nagano 380-8553, Japan. E-mail: tomohiko@shinshu-u.ac.jp; Fax: +81-26-269-5424; Tel: +81-26-269-5414*
[b] *Technical Division, Shinshu University, Wakasato 4-17-1, Nagano 380-8553, Japan.*

† Electronic Supplementary Information (ESI) available: SEM image of the pristine silica fiber (Fig. S1), a cross-sectional TEM image of F15q (Fig. S2), XRD pattern and SEM image of the F15h fibers (Fig. S3), XRD patterns and SEM images of the F50h fibers and the particles, which precipitated during the F50h synthesis (Fig. S4), SEM images of the precipitated particles formed by the F15e and F50e fabrications (Fig. S5), MB breakthrough curves and the adsorption isotherms on Hect-coated fiber samples (Fig. S6), XRD pattern and SEM image of the FDq fibers (Fig. S7). See DOI: 10.1039/x0xx00000x

inorganic polymer, crystallizes directly on spherical, monodisperse amorphous silica particles through hydrothermal reactions.[23,24] Hect layered silicates[34–38] including Laponite®, supplied by conventional homogeneous nucleation reactions, have been widely investigated for their application as adsorbents,[39] dye-supports,[40] sensors,[41,42] photonics,[33,43] column packing materials,[44] and polymer-clay hybrid gels.[45,46] In addition to spherical substrates, silica substrates (e.g., plate, fiber, and monolith) are versatile in shape and morphology; hence, they are expected to exhibit greater applicability for hybrid systems.

Here, we develop a Hect fine crystal, which has been applied as a functional unit in hybrid materials to the surface of a commercially available silica fiber filter disc. The intercalation chemistry of firmly immobilized Hect on the fiber will be discussed through cation-exchange reactions with several metal cations and cationic dyes in batch and flow experiments. In addition, the variation in the negative charge density of the Hect layer has been examined to determine the difference in the adsorption capability of caffeine in water.

Experimental Section

Materials and methods. The Hect crystals were grown on a glass fiber filter disc (ADVANTEC GB-100R, diameter of 90 mm, thickness of 0.38 mm, mass of a sheet: 0.6 g, SiO_2 95 wt%.; the Scanning electron micrographic (SEM) image is shown in the electronic supplementary information (ESI), Fig. S1) through a simple hydrothermal reaction with LiF (Wako Pure Chemical Ind., Ltd.) and $MgCl_2$ (Wako Pure Chemical Ind., Ltd.), accompanied by the hydrolysis of urea (Wako Pure Chemical Ind., Ltd.). A typical molar ratio of LiF:$MgCl_2$:SiO_2:urea in the starting solution was 0.21:0.8:8:2. The amounts of Li and Mg salts added, relative to the amount of SiO_2, were decreased to 15% from a Li:Mg:Si ratio of 1.4:5.6:8.0.[38] The filter paper disc was immersed into a Teflon-lined autoclave containing an aqueous solution of LiF, $MgCl_2$, and urea (125 mL), and then heated at 373 K for 48 h. After the reaction vessel had been cooled in an ice bath, the resulting paper disc was saved in the resulting solution within a short period (a few days) at room temperature without being dried; only characterizations via X-Ray powder diffraction (XRD), SEM, and Transmission electron micrographic (TEM) analyses were conducted under dry conditions. The stocked filter samples were washed with water before using following adsorption experiments. Hereafter, the resulting disc is abbreviated as F15q. "15" and "q" refer to the estimated portion of Hect amount in the disc and the molar ratio of urea to SiO_2 in the initial solution (q: quarter, h: half, and e: equal), respectively. The different molar ratios of LiF:$MgCl_2$:SiO_2:urea are summarized in Table 1. Precipitated particles in the reaction vessel were collected for XRD and SEM analyses.

Cation-exchange capacity (CEC). The CEC of the resulting F15q filter disc was determined from the amount of calcium exchanged.[47] A sheet of the resulting disc was immersed in a $CaCl_2$ (Wako Pure Chemical Ind., Ltd.) aqueous solution (5 mM, 100 mL). The solution was regenerated twice and used after washing with deionized water until a negative $AgNO_3$ test was obtained. The Ca-exchanged form was repeatedly washed with an aqueous solution of NaCl (10 mM, 100 mL) in order to replace $2Na^+$ with Ca^{2+}. The resulting supernatant was used for determining the concentration of Ca^{2+} using ion chromatography. The value of CEC was compared with that using an ASTM (Standard Test Method for Methylene Blue Index of Clay).[48]

Adsorption of methylene blue (MB) from aqueous solution.

The adsorption of cationic MB dye (Wako Pure Chemical Ind., Ltd.) was conducted by both batch and flow tests. The batch experiment was performed as follows: micronized filter disc samples (0.05 or 0.1 g) were reacted with 25 mL of aqueous MB solution (0.13–2.1 mM) in a glass vessel by reciprocal stirring for 1 day at 298 K. To estimate the adsorption of MB to the vessel, blank samples containing 25 mL of aqueous MB solution without the solid sample were also prepared. After centrifugation (1400 g, 20 min), the concentration of MB remaining in the supernatant was determined by visible spectroscopy (λ = 665 nm) to obtain the adsorption isotherm.

The flow experiment was conducted by continuous permeation of an aqueous MB solution (1.0 mM) into the sampled and pristine filter discs with the flow rate of 10 mL/min (space velocity (SV) of 4 min^{-1}) to obtain the breakthrough curves.

Exfoliation test of Hect on the silica fibers. A sheet of the filter disc sample (0.65 g of F15q) was immersed in a LiCl (Wako Pure Chemical Ind., Ltd.) aqueous solution (100 mL, 12 mM) for three weeks at room temperature. A commercially available hectorite (Laponite® XLG) was also used for comparison and 0.15 g of Laponite® was allowed to react with the LiCl aqueous solution for three weeks, followed by titrating an aqueous solution of MB with an appropriate volume to estimate the amount of the layered silicate dispersed in the LiCl solution. The amount of the layered silicate was estimated from a color change of the supernatant from colorless to blue.

Adsorption–desorption of Eu(III) ions. A filter disc sample was allowed to react with $EuCl_3$ (Wako Pure Chemical Ind.,

Table 1. Summary of the MB adsorption results.

Sample (Li:Mg:Si:urea)	BET monolayer capacity [mmol/g]	Breakthrough curve	
		capacity [a] [mmol/g]	time [b] [min]
F15q (0.21:0.8:8:2)	0.08	0.10	7.5
F15h (0.21:0.8:8:4)	0.10	0.12	10
F15e (0.21:0.8:8:8)	-	0.13	10
F50h (0.70:2.7:8:4)	0.16	0.11	12
F50e (0.70:2.7:8:8)	0.20	0.11	12

a: the breakthrough capacity [mmol/g of sample] was calculated by using the following equation: breakthrough capacity = $(c_0–c)ut_b/W$, where c and c_0 are the concentrations [mmol/L] of the effluent and influent, respectively; W is the mass of the sample [kg]; t_b is the breakthrough time [min]; u is the linear flow rate [mL/min]. *b*: the breakthrough time was determined when c_0/c was less than 0.1.

Ltd.) aqueous solution (20 mL, 2 mM) for 24 h at 298 K. The solvent was decarboxylated by bubbling N_2 before the preparation of aqueous $EuCl_3$ solution. The amount of Eu^{3+} adsorbed on the sample was determined by ICP–AES analysis from the difference in the supernatant concentration before and after the adsorption of Eu^{3+}. In order to verify regeneration, the sample was immersed in 20 mM of a NaCl aqueous solution for 3 h, which was then repeated three times.

Adsorption of caffeine on BA-modified fibers from aqueous solution. Immobilization of benzylammonium (BA) into the interlayer space of Hect was conducted by cation-exchange reactions[49] as follows. The crushed filter disc (0.3 g) was mixed with an aqueous solution of BA–HCl (25 mL in 3.6 or 7.2 mM) for 1 day by magnetic stirring at room temperature. The resulting solids were repeatedly washed with deionized water until a negative $AgNO_3$ test was obtained. The solid products were collected by centrifugation (1400 *g* for 15 min) and dried at 323 K following the caffeine adsorption test.

Caffeine (Wako Chemical Industries, Ltd.) was used without further purification and poured into water to prepare an aqueous caffeine solution (0.051–2.1 mM). The crushed disc powder (0.05 g) was mixed with 10 mL of the aqueous caffeine solution by reciprocal stirring for 1 day at 298 K. After centrifugation (1400 *g* for 15 min), the sample was filtered (Merck Millipore, Millex-GP Filter, 0.22 μm, PES) to separate the adsorbents from the supernatants. The concentration of caffeine remaining in the supernatant was determined by HPLC.

Instruments. XRD patterns were obtained by a Rigaku RINT 2200V/PC diffractometer (monochromatic Cu Kα radiation) operated at 20 mA and 40 kV. Nitrogen adsorption–desorption isotherms were measured at 77 K on a Belsorp–mini (BEL Japan, Inc.). Before the adsorption experiment, the samples were heat-treated at 393 K under reduced pressure. SEM images were captured on a Hitachi SU-8000 field-emission scanning electron microscope (operated at 1 kV) after applying an osmium plasma coating to the samples. TEM observations were conducted using a Hitachi HighTech HD-2300A scanning transmission electron and JEOL JEM–2010 TEMs, which have an accelerated voltage of 200 kV. UV–Vis spectra were recorded on a Shimadzu UV–2450PC spectrophotometer. HPLC analysis was conducted on a JASCO LC–2000 Plus equipped with a UV–Vis detector (λ = 275 nm) by using an octadecylsilane column (Mightysil RP–18) at 313 K. ICP–AES was performed using a Hitachi-HighTech SPS5510 spectrometer. Photoluminescence microscopic images were captured using an Olympus BX51 Epi-fluorescence microscope. Ion chromatography was performed on a Shimadzu Prominence HIC–SPNS ion chromatograph.

Results and discussion

SEM images of the pristine silica fiber and F15q filter disc are shown in Fig.s 1a and 1b, respectively. The F15q fibers are evenly coated with very fine particles without the bare surface on silica fibers, as shown in the SEM image. The XRD pattern of the F15q filter disc (Fig. 1c) exhibits reflections of hectorite at 35° (2θ) for (*130*) and 61° (2θ) for (*060*), indicating that the fine crystals in F15q are Hect. The 00*l* reflections were not observed probably due to the poor crystallinity along the *c*-axis

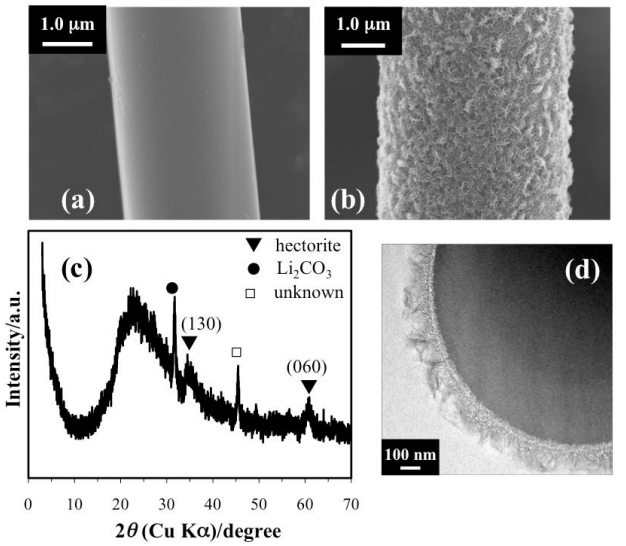

Fig. 1 SEM images of (a) the pristine silica fiber and (b) F15q sample. (c) XRD pattern. (d) a cross-sectional TEM image of F15q.

of the layered silicate. A cross-sectional TEM image in Fig. 1d shows that the thickness of the silicate layers is approximately 0.1 μm and protrusions of silicate layers (several tens of nanometers) develop perpendicularly toward the fiber substrate. The dense silica fiber substrate is partially eroded, and a low-density amorphous substance about 10-nm thick was observed between the dense silica substrate and the layer aggregate (the magnification image is shown in the ESI, Fig. S2), suggesting that the Hect grew from/on a low-density substance. The thickness of the Hect aggregate was approximately 0.1 μm. The Branauer–Emmett–Teller (BET)[50] surface area of F15q was 105 m^2/g, which is larger than that of the pristine silica (<1 m^2/g). The increase in the surface area was due to the formation of fine Hect on the fiber silica, considering that the surface area of Hect is 290 m^2/g when prepared through homogeneous nucleation using silica sol.

Adsorption of the cationic MB dye was examined by batch and flow tests. An aqueous MB solution (1.0 mM) was continuously applied to F15q and the pristine silica fiber filter discs at a flow rate of 10 mL/min (SV of 4 min^{-1}) to obtain the breakthrough curves (Fig. 2a). The Hect fine particles on the fibers did not flow out in the drippings. While the pristine silica did not adsorb MB, the F15q filter well-adsorbed MB within the flow period of 7.5 min, as exemplified in the photograph shown in Fig. 2b. The breakthrough point emerges after 7.5 min, indicating a breakthrough capacity of 0.10 mmol/g (Table 1). If the solution is in full contact with Hect on the disc, this value can be used to predict the monolayer adsorption capacity, because electrostatic interactions of MB with Hect play a dominant role in monolayer adsorption. The BET[50] monolayer capacity of MB for F15q was determined as 0.08 mmol/g (Table 1) according to the adsorption isotherm of the aqueous

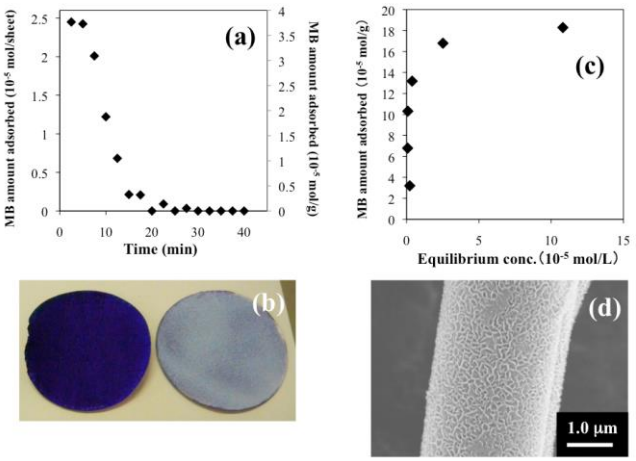

Fig.2 (a) Breakthrough curve of MB obtained by plotting the amount of adsorbed MB versus contact time with F15q. (b) Photograph of the filter discs (left: F15q, right: the pristine silica) taken after the flow test. (c) Adsorption isotherm of MB from the aqueous solution on F15q. (d) SEM image of F15q

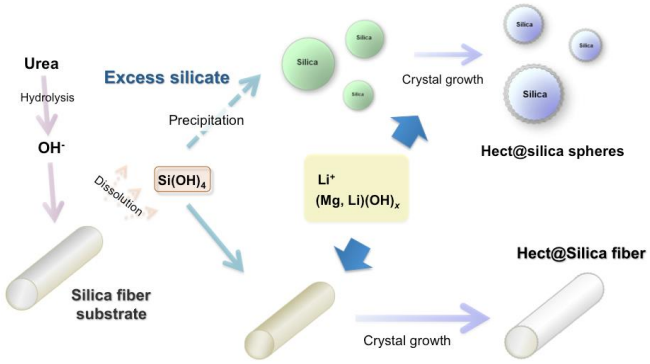

Fig.3 Schematic drawing of the reaction sequence in excess amount of urea.

solution (Fig. 2c). We verified firm adhesion of Hect on the fibers even after the continuous-flow, judging from preserving the surface morphology (Fig. 2d).

Effect of molar ratio on Hect crystallization in the starting solution. When the urea added was doubled, both the monolayer and breakthrough MB capacities of F15h (Table 1) slightly increased (XRD pattern and SEM image of the F15h fibers are shown in the ESI, Fig. S3). When the LiF and $MgCl_2$ quantities were increased to 0.70 and 2.7 mol (compared to 8 mol of SiO_2), respectively, the monolayer MB capacity (F50h: 0.16 mmol/g) was nearly doubled compared to F15h. Since the smaller breakthrough capacity of the thick Hect (0.11 mmol/g) was less than its equilibrium monolayer capacity (0.16 mmol/g), it could not be used in the present continuous-flow MB adsorption (SV of 4 min^{-1}). We deduce that excess soluble silica hydrothermally generated by the excess urea was used for reactions with Li and Mg to generate the thick Hect on the fiber. Upon the synthesis of F50h, spherical particles of approximately 0.2 μm were formed in small quantities both on the fiber filter paper and in the precipitates, as determined by the XRD and SEM analyses (the SEM images and the XRD patterns of the F50h fiber and the precipitate particles are shown in the ESI, Fig. S4). Further addition of urea (increasing to 8 mol of urea compared to 8 mol of SiO_2, yielding F15e and F50e samples) resulted in larger Hect-coated spherical particles (approximately 1 μm) precipitated in large quantities below the hydrothermal reaction vessel (the SEM images are shown in the ESI, Fig. S5). We assume that following the reaction sequence as schematically shown in Fig. 3, the extra urea yields an excess amount of dissolved silica to form spherical silica particles, followed by heterogeneous nucleation of Hect on both of the fibers and spheres. In other words, the heterogeneous nucleation reactions of Hect would be slower than the polymerization of silica sol. In addition, a certain portion of the F50e hybrid fibers was broken during the flow test, probably due to a loss of the silica fiber by the dissolution. The breakthrough curves and the isotherms of MB on these fiber samples are summarized in the ESI, Fig. S6. Thus, the added amounts of urea, LiF, and $MgCl_2$, compared to SiO_2, are important for providing the Hect-coated fibers with mechanical strength without any by-product, as exemplified in the F15q fabrication.

Even when the F15q filter disc was immersed in 12 mM of the LiCl aqueous solution (0.1 L) for three weeks, there was hardly any peeling of the silicate layers from the surface of the silica fibers. Fig. 4a shows a SEM image of the F15q captured after the immersion of the LiCl aqueous solution, confirming that the morphology on the F15q fiber surfaces had been maintained. The amount of peeled layered silicates was estimated using an MB titration test. As shown in Fig. 4b, 0.15 g of Laponite® (a commercial hectorite, with a CEC of 0.74 mEq/g) readily dispersed (or exfoliated) in the LiCl solution, followed by precipitation by the MB addition in the range of 10–70% CEC of Laponite®. At an equivalent point

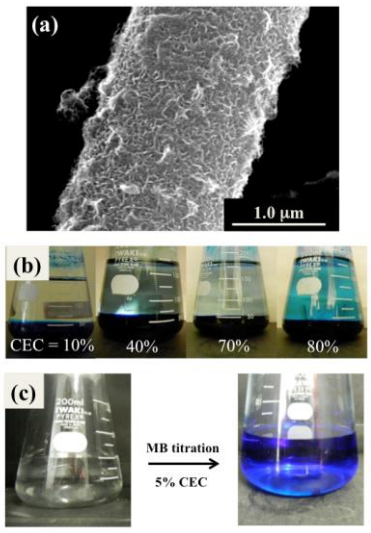

Fig. 4 (a) SEM image of the F15q fiber after immersing LiCl aqueous solution (12 mM) for three weeks. (b) Photographs of Laponite® in the aqueous LiCl solution containing MB with 10–80% CEC of Laponite®. (c) Photographs of the supernatant obtained by F15q immersion in the LiCl aqueous solution before (left) and just after (right) MB was added with 5% CEC of the layered silicate.

(approximately 80% CEC), the color in the supernatant

changed from colorless to blue, meaning that at least 0.12 g (= 0.15 × 0.8 g) of hectorite dispersed in the LiCl solution. In contrast, in the case of F15q, a very small amount of the layered silicates dispersed in the supernatant. When the MB solution was added with 5% CEC, the solution color changed to blue, as shown in Fig. 4c, indicating that less than 0.01 g (7% of Hect in F15q) of the layered silicate peeled off. Therefore, Hect microcrystals were clearly shown to be immobile on the fibers in aqueous media, as already evidenced by the TEM observations (Fig.s 1d and S2).

In order to clarify the ion-exchange ability of Hect in F15q, we employed cation-exchange reactions with Ca^{2+} and Eu^{3+} in water. The cation exchange with Ca^{2+} is a method to determine the CEC.[47] The CEC of F15q was determined to be 0.15 mEq/g, which was close to that (0.18 mEq/g) determined using a ASTM method. We also demonstrate the cation-exchange ability from Eu^{3+} adsorption, because the quantitative ion-exchange reactions in related layered silicates have been reported.[51] The Eu^{3+}-adsorbed adduct was regenerated by immersion in an aqueous NaCl solution, and the procedure was repeated three times. The result is summarized in Fig. 5a. The adsorbed amount on the regenerated sample after the first run was 0.10 mEq/g. Although the amount of Eu^{3+} on the regenerated sample gradually decreased due to strong interactions of Eu^{3+} with Hect compared to Na^+, these cation-exchange reactions on Hect are normal. Luminescence microscope image (Fig. 5b) of the Eu^{3+}-adsorbed F15q clearly shows that the Hect microcrystals grew evenly on the surface of the silica fibers.

Variation in the negative layer charge density of Hect.

Isomorphous substitution of Mg^{2+}–Li^+ in the silicate layer is a factor responsible for determining the layer charge density of Hect, which directly correlates with the CEC. The layer charge density has played an important role in the adsorption

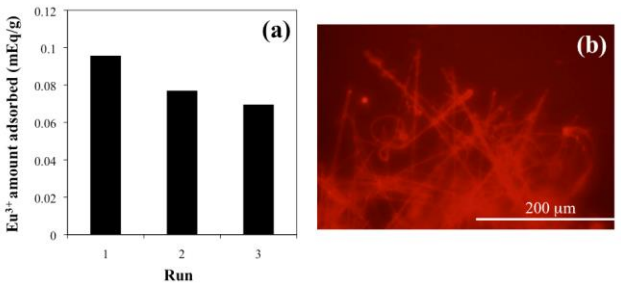

Fig. 5 (a) Change in the amount of adsorbed Eu^{3+} and (b) luminescence microscope image of Eu^{3+}-adsorbed F15q (λ_{ex} = 400–410 nm and λ_{em} > 590 nm).

capability of nonionic organic molecules, because the difference in the spatial distribution (density) of the interlayer organic cations, which depends on the layer charge density, affects the interlayer nanospace created by the organic cations and the silicate layers.[13,15] The CEC (of Hect) varies by changing the amount of LiF added to the starting solution.[38,39] Here, we adopted the molar ratio of Li:Mg = 0.84:0.69 to F15q

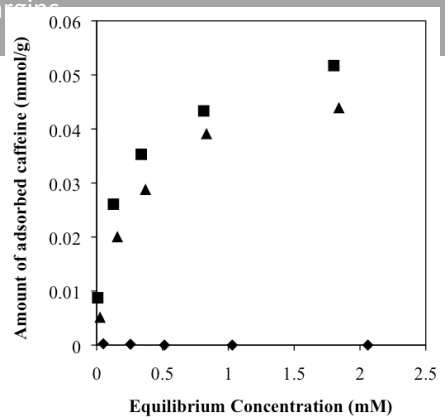

Fig. 6 Adsorption isotherms (298 K) of caffeine from aqueous solution on BA–F15q (squares), BA–FDq (triangles), and the pristine silica fiber (diamonds).

fabrication, in which the filter sample name is denoted as FDq (XRD pattern and SEM image of the F15h fibers are shown in the ESI, Fig. S7). The CEC of FDq determined by the cation exchange with Ca^{2+} increased to 0.47 mEq/g.

We recently found that caffeine is effectively adsorbed on layered silicates (smectites) and the amount of caffeine uptake is affected by the spatial density of BA in the interlayer spaces.[49] The amounts of immobilized BA in F15q and FDq were 0.077 and 0.18 mmol/g, respectively, suggesting the difference in BA spatial density (variation in the interlayer nanospace) in Hect for caffeine accommodation. Fig. 6 shows the adsorption isotherms of the aqueous caffeine solution on BA–FDq and BA–F15q, together with that on a pristine silica fiber. Caffeine adsorbed onto the Hect-coated samples did not adsorb at all on the fiber without BA–Hect, confirming that BA–Hect possesses the adsorption sites of caffeine. The isotherms were fitted to the Langmuir equation[52] given by

$$C_e/Q = (1/K_L Q_m) + (1/Q_m)C_e, \quad (1)$$

where Q_m and K_L are constants related to the maximum adsorbed amount and binding energy, respectively. Q and C_e denote the adsorbed amounts of caffeine and equilibrium concentrations, respectively. The Q_m on BA–F15q was 0.054 mmol/g, which is slightly larger than that on BA–FDq (0.049 mmol/g). Furthermore, the Langmuir constant of K_L = 40 L/g for BA–F15q was larger, compared to that for BA–FDq (22 L/g). BA has created nanospaces that enhance accommodating caffeine molecules, and the exposed siloxane surface in the interlayer space has been recognized as one of the active sites for caffeine adsorption.[49] Larger available nanopores created in the interlayer space of Hect on the fibrous F15q are thought to lead to more effective caffeine uptake. Thus, we empirically showed from the adsorbent fabrication for caffeine uptake that the interlayer nanostructures can be tuned by changing the negative layer charge density (the CEC) of Hect on the fiber silica filter disc. Note that as a merit of Hect, using separation with nanostructural versatility can be applied for practical uses in a flow system.

Conclusions

Cation-exchangeable Hect fine crystals covered thoroughly on a commercially available silica fiber filter paper through

hydrothermal reactions with LiF and $MgCl_2$ in the presence of urea at 373 K for 48 h maintained the disc shape. Hect crystals were firmly immobilized due to heterogeneous nucleation reactions using silica sol, as confirmed by TEM observations and an exfoliation test.

The molar ratio of LiF:$MgCl_2$:urea:SiO_2 in the initial solution was responsible for the negative layer charge density of the Hect crystals, thickness of the Hect shell, mechanical strength of the hybrid fibers, and the presence of by-products as spherical silica particles. In particular, the amount of urea was important for the homogeneous coverage of Hect while preserving the mechanical strength and without forming the precipitates from the silica fiber. In conclusion, a molar ratio of 0.21:0.8:8:2 for LiF:$MgCl_2$:urea:SiO_2 (F15q sample) was sufficient for homogeneous coverage.

The Hect crystals on the filter disc (F15q) show the repeated Na^+–Ca^{2+} and Na^+–Eu^{3+} exchanges. When an aqueous solution of a cationic dye (methylene blue) was penetrated with 4 min^{-1} of SV, the dye adsorbed as monolayer in Hect with a thickness of approximately 0.1 μm. Caffeine adsorbed from the aqueous solution onto the Hect modified with BA via cation-exchange reactions, and the adsorption capability of caffeine (the capacity and affinity of adsorbate–adsorbent) differed from the varied layer charge density of Hect depending on the LiF amount in the starting solution.

The hierarchical hybridization including the interlayer nanostructure of Hect and the microcrystal design was demonstrated on the silica fiber in the present system. The commercially available filter disc applied as the Hect substrate is a reason for developing separation in molecularly recognizable flow systems, both for liquid (chromatography support) and vapor phases (gas separation and catalyst supports), because we can readily select the quartz filter papers based on varied porosity, particle retention, and flow rate for appropriate gas/liquid permeation.

Acknowledgements

This research was funded by JSPS (Grant-in-Aid for Scientific Research, #26810121), The Cosmetology Research Foundation, and JGC-S Scholarship Foundation.

Notes and references

1 M.-C. Daniel and D. Astruc, *Chem. Rev.,* 2004, **104,** 293.
2 D. Michael, Y. Liu and Y. Yin, *Chem. Rev.,* 2014, **114,** 9853.
3 X. W. Lou, L. A. Archer and Z. Yang, *Adv. Mater.,* 2008, **20,** 3987.
4 G. D. Li and Z. Y. Tang, *Nanoscale,* 2014, **6,** 3995.
5 Y. Wang, A. S. Angelatos and F. Caruso, *Chem. Mater.,* 2008, **20,** 848.
6 Q. Zhang, I. Lee, J. B. Joo, F. Zaera and Y. Yin, *Acc. Chem. Res.,* 2013, **46,** 1816.
7 W. I. Park, D. H. Kim, S.-W. Jung and G.-C. Yi, *Appl. Phys. Lett.,* 2002, **80,** 4232.
8 B. Liu and E. S. Aydil, *J. Am. Chem. Soc.,* 2009, **131,** 3985.
9 S. A. Chambers, *Adv. Mater.,* 2010, **22,** 219.
10 M. Ogawa and K. Kuroda, *Chem. Rev.,* 1995, **9,** 399.
11 S. M. Auerbach, K. A. Carrado and P. K. Dutta, (Eds.) *Handbook of Layered Materials;* Marcel Dekker, 2004.
12 G. Rogez, C. Massobrio, P. Rabu and M. Drillon, *Chem. Soc. Rev.,* 2011, **40,** 1031.
13 T. Okada, Y. Ide and M. Ogawa, *Chem.–Asian J.,* 2012, **7,** 1980.
14 M. Chhowalla, H. S. Shin, G. Eda, L. J. Li, K. P. Loh and H. Zhang, *Nature Chem.,* 2013, **5,** 263.
15 T. Okada, Y. Seki and M. Ogawa, *J. Nanosci. Nanotechnol.,* 2014, **14,** 2121.
16 S. Furukawa, J. Reboul, S. Diring, K. Sumida and S. Kitagawa, *Chem. Soc. Rev.,* 2014, **43,** 5700.
17 J. T. Kloprogge, S. Komarneni J. E. Amonette, *Clays Clay Miner.,* 1999, **47,** 529.
18 K. A. Carrado, A. Decarreau, S. Petit, F. Bergaya and G. Lagaly, in *Handbook of Clay Science (Developments in Clay Science, Vol. 1);* F. Bergaya, B. K. G. Theng and G. Lagaly (Eds.) Elsevier; Amsterdam, 2006, pp.115–139.
19 D. V. Bavykin, J. M. Friedrich and W. C. Walsh, *Adv. Mater.,* 2006, **18,** 2807.
20 Z. Liu, R. Ma, Y. Ebina, N. Iyi, K. Takada and T. Sasaki, *Langmuir,* 2007, **23,** 861.
21 M. A. Bizeto, A. L. Shiguiharab and V. R. L. Constantino, *J. Mater. Chem.,* 2009, **19,** 2512.
22 Q. Wang and D. O'Hare, *Chem. Rev.,* 2012, **112,** 4124.
23 T. Okada, S. Yoshido, H. Miura, T. Yamakami, T. Sakai and S. Mishima, *J. Phys. Chem. C,* 2012, **116,** 21864.
24 T. Okada, A. Suzuki, S. Yoshido and H. M. Minamisawa, *Microporous Mesoporous Mater.,* 2015, **215,** 168.
25 T. Okada, M. Sueyoshi and H. M. Minamisawa, *Langmuir,* (manuscript in revision).
26 J. Pérez-Carvajal, P. Aranda, A. Berenguer-Murcia, D. Cazorla-Amorós, J. Coronas and E. Ruiz-Hitzky, *Langmuir,* 2013, **29,** 7449.
27 H. Chen, F. Zhang, S. Fu and X. Duan, *Adv. Mater.,* 2006, **18,** 3089.
28 F. Zhang, L. Zhao, H. Chen, S. Xu, D. G. Evans and X. Duan, *Angew. Chem. Int. Ed.,* 2008, **47,** 2466.
29 T. Zhang, Y. Zhou, X. Bu, J. Xue, J. Hu, Y. Wang and M. Zhang, *Microporous Mesoporous Mater.,* 2014, **188,** 37.
30 K. Inukai, Y. Hotta, M. Taniguchi, S. Tomura and A. Yamagishi, *J. Chem. Soc., Chem. Commun.,* 1994, 959.
31 E. R. Kleinfeld and G. S. Ferguson, *Science,* 1994, **265,** 370.
32 R. A. Caruso, A. Susha and F. Caruso, *Chem. Mater.,* 2001, **13,** 400.
33 B. V. Lotsch and G. A. Ozin, *Adv. Mater.,* 2008, **20,** 4079.
34 K. Torii and T. Iwasaki, *Chem. Lett.,* 1986, 2021.
35 K. A. Carrado, P. Thiyagarajan and R. E. Winans, *Inorg. Chem.,* 1991, **30,** 794.
36 K. A. Carrado, J. E. Forman, R. E. Botto and R. E. Winans, *Chem. Mater.,* 1993, **5,** 472.
37 M. Reinholdt, J. Miehe-Brendle, L. Delmotte, M.-H. Tuilier, R. le Dred, R. Cortes and A.-M. Flank, *Eur. J. Inorg. Chem.,* 2001, 2831.
38 M. Ogawa, T. Matsutomo and T. Okada, *J. Ceram. Soc. Jpn.,* 2008, **116,** 1309.
39 T. Okada, T. Matsutomo and M. Ogawa, *J. Phys. Chem. C,* 2010, **114,** 539.
40 R. Sasai, N. Iyi, T. Fujita, L. F. Arbeloa, M. V. Martinez, K. Takagi and H. Itoh, *Langmuir,* 2004, **20,** 4715.
41 M. R. Kleinfield and G. S. Ferguson, *Chem. Mater.,* 1995, **7,** 2327.
42 D. Shan, C. Mousty and S. Cosnier, *Anal. Chem.,* 2004, **76,** 178.
43 B. V. Lotsch and G. A. Ozin, *J. Am. Chem. Soc.,* 2008, **130,** 15252.
44 Y. Yamagishi, M. Taniguchi, Y. Imamura and H. Sato, *Appl. Clay Sci.,* 1996, **11,** 1.

45 K. Hararuchi, H.-J. Li, K. Matsuda, T. Takehisa and E. Elliot, *Macromolecules,* 2005, **38,** 3482.
46 Q. Wang, J. L. Mynar, M. Yoshida, E. Lee, M. Lee, K. Okuro, K. Kinbara and T. Aida, *Nature*, 2010, **463,** 339.
47 M. Ogawa, Y. Nagafusa, K. Kuroda and C. Kato, *Appl. Clay Sci.,* 1992, **7,** 291.
48 ASTM C 837-09. Standard Test Methods of Methylene Blue Index of Clay, *American Society for Testing and Materials,* 2014.
49 T. Okada, J. Oguchi, K. Yamamoto, T. Shiono, M. Fujita and T. Iiyama, *Langmuir,* 2015, **31,** 180.
50 S. Brunauer, P. H. Emmett and E. Teller, *J. Am. Chem. Soc.*, 1938, **60,** 309.
51 T. Okada, Y. Ehara and M. Ogawa, *Clays Clay Miner.,* 2007, **55,** 348.
52 I. Langmuir, *J. Am. Chem. Soc.,* 1918, **40,** 1361.